JOURNAL OF CATALYSIS 37, 204–214 (1975)

Structure and Catalytic Activity of $MoO_3 \cdot Al_2O_3$ Systems

II. Solid-State Properties of Reduced Catalysts

N. GIORDANO, A. CASTELLAN, J. C. J. BART, A. VAGHI AND F. CAMPADELLI

Montedison, Bollate Research Center
Bollate, Milano, Italy

Received December 6, 1973; revised September 2, 1974

$MoO_3 \cdot Al_2O_3$ catalysts containing up to 30 wt% of the active phase, previously studied in the oxidized state, have been examined by optical reflectance and EPR after treatment in reducing and outgassing conditions. Evidence was found for changes in the nature of the surface structures as a function of the acidity of the support, the molybdenum concentration and conditions of reduction. At the lowest concentrations (up to 4 wt% MoO_3) interaction with the most basic sites of the support leads to the oxyanionic $[Mo^{V}O_4]^{3-}$ form. In the intermediate composition range (4–10 wt%), increased acidity of the support, brought about by progressive depletion of distinct types of surface OH groups of Al_2O_3, gives rise to stabilized Mo(V) in the form of the oxyanionic species $[MoO_4]^{3-}$, $[HMoO_4]^{2-}$ and $[Mo_2O_7]^{4-}$, besides oxycations such as mono- and bis-molybdenyl species, $[MoO(OH)]^{2+}$ and $[Mo_2O_3]^{4+}$. In the molybdenum-rich catalysts polyoxyanions containing Mo(VI) and Mo(V) are found in mild conditions, while Mo(IV) is formed by more drastic reduction. Further, in this region oxycations such as MoO^{3+} are present both at the surface and in the bulk.

INTRODUCTION

The studies reported in Part I (*1*) have indicated that the geometry of coordination of molybdenum in oxidized catalysts varies from predominantly monomeric tetrahedral (in the low MoO_3 region) to octahedral Mo(VI), deposited in polymeric form over the surface or incorporated in the lattice, at higher MoO_3 contents; at still higher MoO_3 concentrations, $Al_2(MoO_4)_3$ is formed containing tetrahedral Mo(VI). In the present paper we report on the structure of these same catalysts after reduction or outgassing. These studies provide the basis for discussion of catalytic performance in some model reactions to be reported in Parts III and IV (*2,3*). Reference to the various samples will be made as MoO_3-x where x indicates the percentage of active element.

EXPERIMENTAL PROCEDURE

ESR measurements were made at room temperature with a JEOL JES ME 1X type spectrometer (X-band) using 100 kHz field modulation. Relative spin concentrations were derived by comparison of the doubly integrated Mo(V) spectral intensities with the strong pitch Varian reference. The g-values were determined by calibration against the fourth line of the Mn-marker, with $\Delta H \approx 87$ gauss.

Samples, prepared as in Part I (*1*), were outgassed in a stream of pure He at 500°C for 2 h, and (a) cooled to room temperature, again in He (outgassed samples) or (b) reduced by a 1:1 flow of $He + H_2$ (total volume 60 $cm^3\ min^{-1}$) at 350°C for 5 h, followed by cooling to room temperature in He (reduced samples). Contact with air was therefore carefully avoided.

To ensure that the ESR signal was proportional to the number of paramagnetic centers per unit volume, care was taken to fill the ESR sample tubes up to a height exceeding the depth of the resonant cavity.

Reduction and reoxidation rates were determined on a TG analyzer (Du Pont 950), under strictly controlled conditions, as follows: a 100–150 mg sample suspended in a gold crucible was heated in dry air (flow-rate: 60 ml/min; heating rate: 15° C/min) to the desired temperature (350, 400, or 500°C). After removal of moisture and outgassing in He until the oxygen level was below 20–30 ppm at the exit of the furnace, as measured by a galvanometric device (*4*), a H_2/He mixture (1:6 or 1:1 molar ratios) was admitted until constant weight (from 2 to 3 h). The reduced samples were then bathed in dry He and reoxidized in air to constant weight. Reported weight changes refer to the MoO_3 content in dried samples; the accuracy was 0.2 mg.

Diffuse reflectance spectra were recorded in the 210–700 nm range on a Perkin–Elmer Hitachi EPS 3T spectrophotometer against an Al_2O_3 standard, after sample preparation in a dry-box.

RESULTS

Electron Spin Resonance

Both reduced and outgassed samples show a signal at $g_1 \cong 1.94$; further, a rather narrow signal at $g_2 \approx 2.01$ is found in MoO_3-poor reduced samples. No ESR signal is observed in outgassed samples below MoO_3-6, but from this composition onwards, the g_1 signal intensity increases with MoO_3-content (Figs. 1a, b). Relative spin concentrations, which reach a maximum around 20 wt% MoO_3 (Fig. 3), are lower in outgassed than in reduced samples at all compositions. The apparent degree of asymmetry also increases with

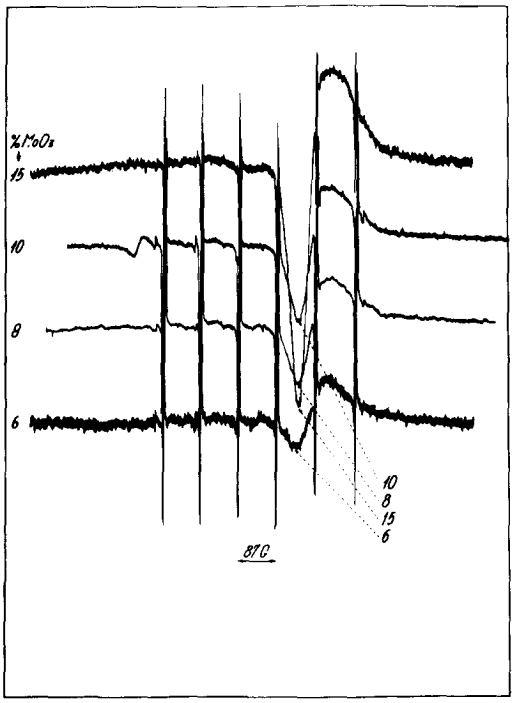

FIG. 1a. EPR spectra of outgassed samples (6–15 wt% MoO_3), against a Mn/MgO marker (see text).

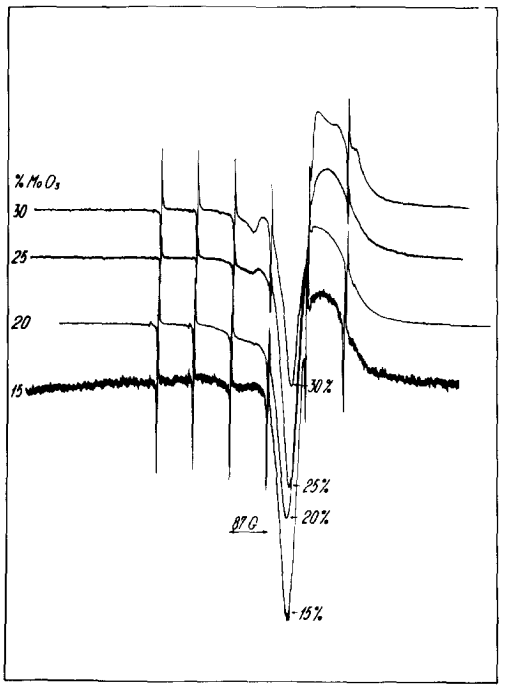

FIG. 1b. EPR spectra of outgassed samples (15–30 wt% MoO_3).

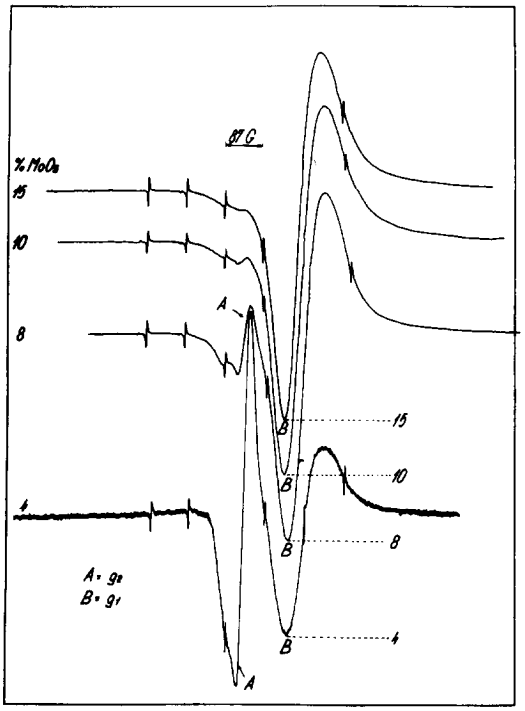

FIG. 2a. EPR spectra of reduced samples (4–15 wt% MoO_3).

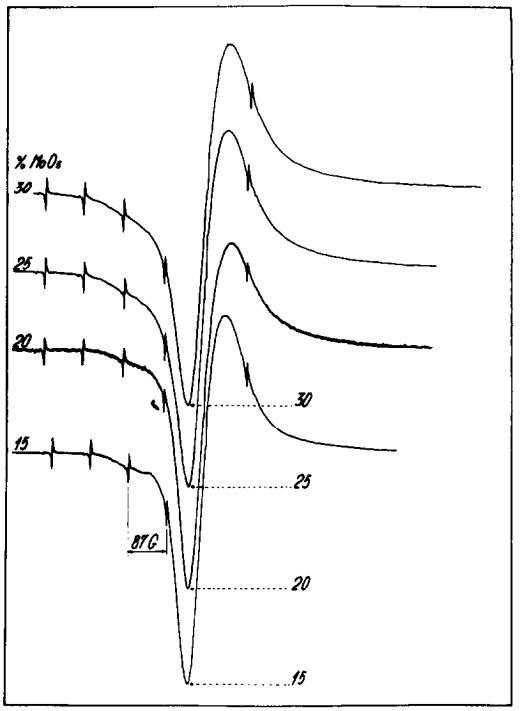

FIG. 2b. EPR spectra of reduced samples (15–30 wt% MoO_3).

MoO_3 concentration and $g_{||}$ and $g_{\perp}$ are well separated at MoO_3-30; spectral parameters are shown in Table 1. In reduced samples the g_2 signal (below 10 wt% MoO_3) is a maximum at MoO_3-4; this signal disappears on admission of O_2 or H_2O. The g_1 signal, observed over the whole range of compositions, is similar to that found in outgassed samples, but is apparently less asymmetric (Figs. 2a, b). Relative spin concentrations per *unit weight of support* calculated over g_1 and g_2 vary with composition and exhibit relative maxima at MoO_3-10 and MoO_3-25. Figure 3 clearly indicates two distinct Mo(V) regions in reduced samples (curve *a*) as opposed to one in outgassed specimens (curve *b*). On the basis of the spin concentration per *unit weight of* MoO_3, the twin peak of the g_1 signal turns into a single one with a maximum around MoO_3-10 (Fig. 4). With regard to spin concentration, an estimate based upon strong pitch values leads to about 10^{17} spins/g of catalyst, corresponding to a small fraction of all Mo present in the catalyst only, and also much lower than that expected from reduction experiments (valence state of Mo at 350°C is 5.7–5.4).

TABLE 1
EPR PARAMETERS DERIVED BY SPECTRAL SIMULATION

		g		$\Delta H_{1/2}$ Gauss		
% MoO_3	Treatment	⊥	//	⊥	//	Line shape
10	Outgassing	1.94	1.89	~ 75	~100	Lorentzian
20	Outgassing	1.95	1.90	~ 65	~ 80	Lorentzian
30	Outgassing	1.94	1.88	~ 65	~ 80	Gaussian
10	Reduction	1.94	1.88	~ 75	~100	Gaussian
30	Reduction	1.94	1.90	~100	~140	Lorentzian

The characteristics of the spectra (Table 1) prove the presence of Mo(V), which is typically described by $g \cong 1.94$ (*5–7*); anisotropic g-values also indicate that Mo(V) is in an electrical field of pyramidal or axially distorted tetrahedral

symmetry, in good agreement with literature data (7–10).

Reduction–Oxidation

Results of reduction and reoxidation experiments are summarized in Table 2. On reduction, formal valence states gradually fall with increasing MoO_3 concentration; while lower T and p_{H_2} favor reduction to Mo(V), under more severe conditions (i.e., high T) valence levels such as (III) and (IV) are reached. It would appear from optical microscopy that metallic Mo is present together with Mo(IV) or a higher oxidation state; no evidence was found for Mo(III) ions. The catalysts also vary in reduction rates which increase with MoO_3 content; the variation is particularly pronounced at the most severe conditions ($T = 500°C$, $p_{H_2} = 0.5$ atm). With regard to reoxidation, MoO_3-poor catalysts are the most difficult to reoxidize, both in terms of degree and rates; this behaviour is most pronounced at lower temperatures.

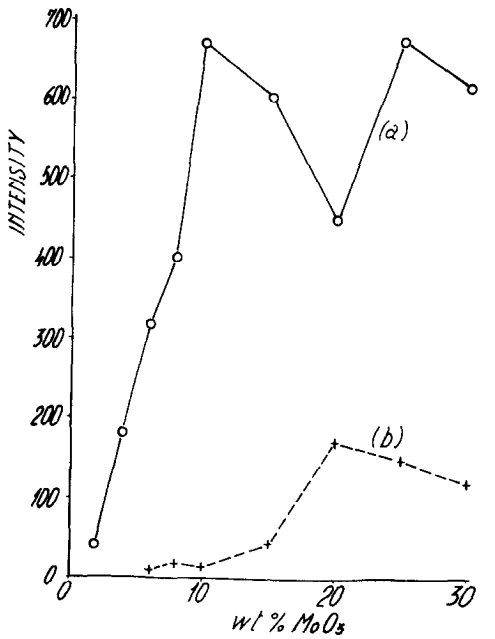

FIG. 3. Relative integrated intensity of g_1 and g_2-signals per gram support, as a function of the composition (arbitrary scale). (a) reduced samples. (b) outgassed samples.

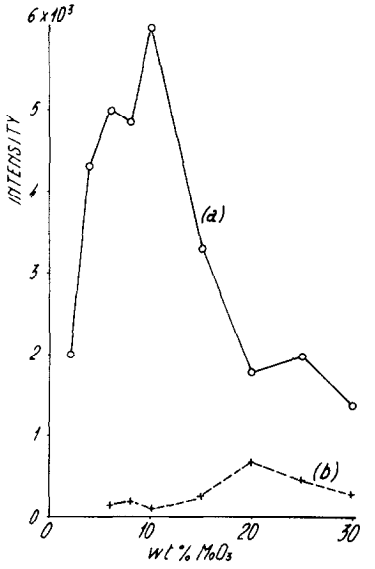

FIG. 4. Relative integrated intensity of g_1 and g_2-signals per gram MoO_3, as a function of the composition and expressed on the same arbitrary scale as Fig. 3. (a) reduced samples, (b) outgassed samples.

Electronic Spectra

Reduced samples. Comparison of the electronic spectra of reduced samples (Table 3a) with those of fresh catalysts (see Fig. 4 in Part I (*1*), shows the profound structural modifications on reduction; abrupt changes are observed at 15 wt% MoO_3 and point to two distinct regions. Below MoO_3-15 reduction leads to strong absorption around 300 and 400 nm, besides the unchanged 250–270 nm absorption; a shoulder at 500 nm (MoO_3-2) overlaps with the 400 nm band at higher MoO_3 compositions to give a broad band. The position of the maximum of the 300 nm band gradually shifts from 290 to 330 nm, with increasing MoO_3 contents; also, the intensities of the 300 and 400–500 nm bands rise up to MoO_3-10. Afterwards, the spectra change drastically, showing generally lower intensity at 270–330 nm, a very broad band in the 400–500 nm range and a diffuse band between 600 and 700 nm.

The 250–270 nm absorption is ascribed

TABLE 2
VALENCE LEVELS OF MOLYBDENUM, AND REDUCTION AND REOXIDATION RATES[a]

Catalyst[d]	Reduction				Reoxidation		
	T_R	p_{H_2}	$V_R{}^b \times 10^{-4}$	Valence state	T_{OX}	$V_{OX}{}^c$	Fraction reoxidized
MoO_3-8	350°C	0,167	1,08	5,70	350°C		37,5%
MoO_3-10	350°C	0,167	2,32	5,65	350°C	0,018	66,5%
MoO_3-15	350°C	0,167	2,63	5,34	350°C	0,047	81,5%
MoO_3-20	350°C	0,167	10	5,05	350°C	0,037	88,5%
MoO_3-10	350°C	0,50	5	5,39	350°C	0,002	98,0%
MoO_3-15	350°C	0,50	11	5,24	350°C	0,033	100%
MoO_3-20	350°C	0,50	27,5	4,81	350°C	0,040	88%
MoO_3-25	350°C	0,50	14,1	4,70	350°C	0,043	91,4%
MoO_3-30	350°C	0,50	15,4	4,35	350°C		
MoO_3-4	400°C	0,50	12,12	5,25	400°C	0,048	83,5%
MoO_3-6	400°C	0,50	9,70	5,40	400°C	0,050	91,2%
MoO_3-15	400°C	0,50	47,6	4,78	400°C	0,054	95,1%
MoO_3-20	400°C	0,50	41,7	4,63	400°C	0,047	92,7%
MoO_3-25	400°C	0,50	58,9	4,24	400°C	0,055	96%
MoO_3-4	500°C	0,50	26,9	5,18	500°C	0,030	100%
MoO_3-10	500°C	0,50	38,4	4,75	500°C	0,067	99,5%
MoO_3-15	500°C	0,50	64,5	4,32	500°C	0,076	100%
MoO_3-20	500°C	0,50	83,5	3,98	500°C	0,075	100%
MoO_3-25	500°C	0,50	125	3,50	500°C	0,074	100%
MoO_3-30	500°C	0,50	166	3,26	500°C	0,054	99,6%
Al-Mo-700	500°C	0,50	37,1	2,53	500°C	0,02	23,5%
Al-Mo-500	500°C	0,50	50,0	3,27	500°C	0,08	93%

[a] In reduction experiments a 120′ time lag was used as reference.
[b] V_R = rate of reduction, expressed as g O_2 lost/g MoO_3 min^{-1}.
[c] V_{OX} = rate of reoxidation, expressed as g O_2 absorbed/g MoO_3 min^{-1}.
[d] Calcined at 500°C for 8 hr, unless indicated otherwise.

TABLE 3a
REFLECTANCE SPECTRA OF REDUCED MoO_3·Al_2O_3 SAMPLES

Samples	Position of the bands (nm)					Observations
MoO_3-2-500	250 sh	290	425	500		(1) Diffuse absorption in the visible increases with increasing MoO_3
MoO_3-4-500	255	285 sh	420 br	[500 sh][a]		
MoO_3-6-500	260	295	400 sh br	[540 sh]		
MoO_3-8-500	270 sh	305	400 sh br	[500 sh]		(2) Intensity of the band at ~700 nm reaches a maximum at the MoO_3-30 composition
MoO_3-10-500	270 sh	330	410	[500 sh]		
MoO_3-15-500	270 sh		420 sh	480	620 sh[b]	
MoO_3-20-500		290 sh	410		620 sh[b]	
MoO_3-25-500		290 sh	430		640–680[b]	
MoO_3-30-500		290 sh	440		640–680[b]	

[a] [ ] Band not well defined, due to overlapping with the band at ~400 nm.
[b] These bands shift to higher λ (~700 nm) on exposing samples to air.

TABLE 3b
REFLECTANCE SPECTRA OF OUTGASSED $MoO_3 \cdot Al_2O_3$ SAMPLES

Samples	Position of the bands (nm)				Observations
MoO_3-8-500	270–280		420–480[b]	—	Both the diffuse absorbance in the region 400–500 nm and the intensity of the band at 700 nm reach a maximum at MoO_3-25.
MoO_3-15-500	290	300[a]	400–600[b]	~700	
MoO_3-20-500	280 sh	315[a]	420–540[b]	~700	
MoO_3-25-500	280 sh	322[a] ↓	400–540[b] ↓	~700 ↓	
MoO_3-30-500	265	290–310[a] ↑	420–540[b] ↑	~700 ↑	

[a] This band is composite and hence difficult to locate precisely.
[b] Absorption in the interval 400–540 nm is diffuse.

to tetrahedral Mo(VI) (*11–13*). As to the 300–330 nm band, attribution to octahedral Mo(VI) is rejected because of the increasing intensity of the band after reduction; the band is thus assigned to reduced species (see below: Table 4, Refs. (*14–23*)). Considering absorption bands separately, reduced Mo is thus apparent from the 500 nm band of Mo(IV) in a distorted octahedral coordination (*21*) or of Mo(V) in monomeric form (*13,14*); Mo(V) in a C_{4v} or O_h symmetry is also suggested by the 400 nm band (*11,13*). However, the simultaneous occurrence of the 270, 330, 400 and 500 nm bands in the low MoO_3 range after reduction suggests a complex surface structure; comparison with spectra of reference compounds (Table 4) indicates bis-molybdenyl-like structures as in the $Mo_2^{V}O_3(acac)_4$ complex (18), which is octahedral.

As to the MoO_3-richer catalysts (Table

TABLE 4
REFLECTANCE SPECTRA OF MODEL COMPOUNDS

Model compound	λ_{max} (nm)					Observations	Ref.
$Mo(OH)_3(acac)_2 \cdot 3H_2O$[a]			490			Mo^{5+}, monomer	(*14*)
$Mo_4O_{10}(OH)_2$		373			690	Mo^{6+}-Mo^{5+} in square pyramid configuration	(*15*)
$P_2Mo_{18}O_{62-x}^{6-}$					600–750	Position of the band varies with degree of reduction (Mo^{5+})	(*16*)
$Mo_2O_3(acac)_4$[a]		327	400(sh br)[b]	485		Pairs of Mo^{5+} bound through Mo–O–Mo bonds	(*17*)
$Mo_2O_3(acac)_4$[a]	263–287	320–30	405	490	(750)	Position at 750 nm is attributed to the transition (acac → Mo^{5+})	(*18*)
$[MoOCl_5]^{2-}$			445		712	Mo^{5+} in highly distorted tetragonal coordination	(*19*)
$MoOPO_4$		380			700	Mo^{5+} in square pyramid configuration	(*20*)
MoO_2			500 (br)			$[Mo^{4+}O_6]$ in a highly distorted octahedron	(*21*)
$MoCl_3$			518			Mo^{3+}	(*22*)
$Mo^{III}(acac)_3$[a]		370	~430(sh br)			Mo^{3+} in octahedral coordination	(*23*)

[a] (acac) = acetylacetonate.
[b] Intense owing to nearby charge transfer band.

3a), results of reduction experiments (Table 2) and the attribution of the 500 nm band to Mo(IV) (Table 4), indicate that variations in the spectra should be assigned to a gradual increase in Mo(IV). Furthermore, the broad band in the 600–700 nm region appears to arise from structures such as $Mo_4O_{10}(OH)_2$, characterized by mixed Mo(VI) and Mo(V) in square-pyramidal configurations, or reduced heteropolyacids of the type $[P_2Mo_{18}O_{68-x}^{6-}$(Table 4). Moreover, as the position of the maximum shifts from 620 to 680 nm as the MoO_3 content increases, a gradual increase of degree of reduction (higher Mo(V)/Mo(VI) ratios) is suggested. Considering the 600–700 and 400 nm bands together, Mo(V) in structures containing the MoO^{3+} ion, i.e. like $MoOPO_4$, appear possible as well.

Outgassed samples. Spectra of outgassed samples (Table 3b) are typically described by the MoO_3-8 and MoO_3-25 samples. In the former case, the spectra are very similar to those of oxidized samples with a single absorption band at 270 nm and some diffuse absorption at 400–500 nm. The MoO_3-25 sample has the 270 and 330 nm bands in common with oxidized samples, and shows diffuse absorption around 500 nm and strong absorption at 700 nm. The intensity of this band increases with the MoO_3 concentration up to MoO_3-25 and then decreases.

Spectral evidence, together with ESR results, indicates that coordination geometries already present in the oxidized samples (270 and 330 nm) remain almost unchanged on outgassing; the presence of the 500 and 700 nm bands at the highest MoO_3 range indicates that octahedral configurations have been partly transformed into structures containing both Mo(VI) and Mo(V), as in reduced samples. At the mild experimental conditions of outgassing, the structures are likely to

TABLE 5

			Outgassed[a]			Reduced[a]			
			Low MoO_3 region		High MoO_3 region	Low MoO_3 region		High MoO_3 region	
Technique	Attribution	Symmetry	(2–4%)	(6–15%)	(15–30%)	(2–4%)	(6–15%)	(15–30%)	Model compounds
Optical reflectance									
270 nm	Mo(VI)	tetrahedral	x	x	low	x	x	—	$(MoO_4)^{2-}$
330 nm	Mo(VI)	octahedral	—	x	x		x	low	$Mo_7O_{24}^{6-}$
400 nm	Mo(V)	C_{4v} octahedral	—	low	low	x	x	x	
500 nm	Mo(V)		—	low	low	x	x	x	$MoO(OH)(acac)_2$
	Mo(IV)	distorted octahedral						x	MoO_2
600–750 nm	Mo(VI) + Mo(V)	square pyramid	—	very low	x	low	—	x	$P_2Mo_{18}O_{68-x}^{6-}$
270, 330, 400 nm 500 nm	Mo(V)dimer	octahedral					x	—	$Mo_2O_3(acac)_4$
380,700 nm	Mo(VI) + Mo(V)	square pyramid						x	$Mo_4O_{10}(OH)_2$
	Mo(V)							x	$MoOPO_4$
450,700 nm	Mo(V)	octahedral tetragonally distorted						x	$(MoOCl_5)^{2-}$, MoO^{3+}
Reduction (T = 350°C) or outgassing (T = 350°C) EPR			—	—	Mo(V)	Mo(V)	Mo(V)+ Mo(IV)	Mo(V)+ Mo(IV)	
			—	g_1	g_1	g_1,g_2	g_1	g_1	

[a] x = present; — = absent.

originate from polymeric chains by random rupture of bridged oxygen bonds rather than terminal oxygens, thus leading to either monomeric Mo(V) (500 nm) or polymeric mixed Mo(VI)/Mo(V) species (600–700 nm), as follows:

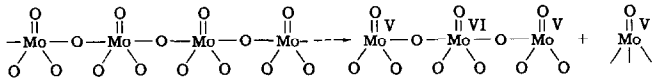

The differences in the solid state properties of the various catalysts are summarized in Table 5.

DISCUSSION

The results presented indicate two distinct regions of surface structure, respectively below and above the composition MoO_3-15. The discussion is therefore divided into two parts, including both outgassed and reduced samples.

Low MoO_3-region. Reduction experiments show a linear decrease of Mo-valence states as a function of the MoO_3-concentration (Table 2); among these, Mo(V) has been revealed by ESR and reflectance spectra, in agreement with some previous reports (*5–8,11,24,25*). In the literature, the nature of these stabilized Mo(V) species is still controversial. Masson (*24*) suggests that Mo(V) derives from surface species formed by interaction between monolayer MoO_3 and the support. It has also been claimed that Mo(V) originates from $Al_2(MoO_4)_3$ (*8,11,25*) or from $[MoO_6]$ occupying octahedral vacancies of the Al_2O_3 support (*6,26*); the latter interpretation is based on observed dissimilarities in samples supported on η or γ-Al_2O_3. According to Seshadri (*5*), Mo(V) is due to MoO^{3+} species stabilized by coordination with surface atoms.

The present results, while confirming some general features already reported, allow further conclusions with regard to the debated question. In the low MoO_3 region, given the essentially tetrahedral nature of the precursors in the oxidized samples, it is reasonable to suppose, by analogy with the behavior of chromium on similar supports, that in the course of the reduction structures of the type

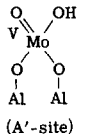

(A′-site)

are formed which imply Mo(V) bound to the most basic sites of the Al_2O_3 support. These A′-like structures reasonably explain the slight weight gain of the samples up to 4 wt% MoO_3 during the initial stages of reduction, by analogy with Dollimore and Rickett (*27*), and the rates of reduction and reoxidation (Table 2). At lower MoO_3 contents, the high fraction of isolated tetrahedra with doubly-bonded oxygens as compared to the polymeric MoO_3 species with bridged oxygens (high MoO_3 region) explains not only the greater resistance to reduction but also the greater difficulty in reoxidation, which probably comes about from competition between O_2 and residual water retained on the solid after the reduction step. In accordance with the behaviour towards coordinatively unsaturated tetrahedral ions of various transition metals (*28*), the stronger chemisorption of water may justify the impediment to reoxidation of reduced catalysts. The observed g_2 signal in reduced samples in the lowest MoO_3 region disappears on admission of O_2 or water and may be taken as an indirect confirmation of the existence of quasi-isolated tetrahedra which change their characteristics upon chemisorption of H_2O.

As the MoO_3 concentration increases from 4 to 10–15 wt%, the nature of the

catalysts changes, as indicated by: (a) the progressive drift of the ~ 300 nm band from 290 to 330 nm (Table 3a) and (b) the increasing intensity of all characteristic absorption bands (270, 330, 400, 500 nm) of bis-molybdenyl-like structures reaching maximum values at MoO_3-10 and dropping sharply at MoO_3-15.

The intensity of the Mo(V) ESR signal has a similar behavior (Fig. 3), indicating eventually a structural correlation. The ESR signal might be related to the described bis-molybdenyl-structures; this attribution appears less likely, since at room temperature these dimeric structures are almost diamagnetic (*5*). Therefore, other true paramagnetic species are to be invoked. While a definite answer to the question must await an accurate study of the variations in the ESR signal intensity as a function of the temperature, the observed variations of the line shape with concentration appear to favor monomeric rather than dimeric species. Thus, it appears that the ESR signal intensity does not simply represent a direct measure for the total number of Mo(V) centers. On the whole, spectroscopic and ESR results point to a simultaneous increase of dimeric and monomeric species towards higher MoO_3 content. With regard to monomers, one may expect, besides the $[MoO_4]^{3-}$ (A′-site) form, singly protonized forms involving only one Al center per Mo atom, as:

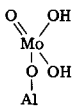

(A″-site)

coordinated in the anion as $[HMoO_4]^{2-}$, or as the cation $[MoO(OH)]^{2+}$ (A‴ -site). Similarly, the dimeric Mo(V) species, well asserted on the basis of reflectance spectra, can be regarded either as bis-molybdenyl-like structures $[Mo_2O_3]^{4+}$ (B′-type) or as reduced dimolybdate structures, such as

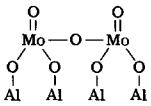

$[Mo_2O_7]^{4-}$
(B″-site)

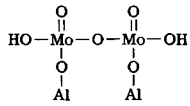

$[H_2Mo_2O_7]^{2-}$
(B‴-site)

Both of them can be described as derivatives of A′ and A″ sites through intermolecular dehydration or step-wise reduction of the precursors in the oxidized samples. Concluding, we may state that: (*a*) the ESR signal measures paramagnetic monomeric sites (A′, A″ and A‴), (*b*) reflectance spectra and reduction experiments give also information about dimeric species (B′, B″ and B‴ sites), (*c*) monomeric and dimeric species reach maximum concentrations at MoO_3-10 with a prevailing trend to dimeric structures.

High MoO_3 region. The higher rates of reduction, the increasing Mo(IV) fraction (Table 2), and the complete reoxidation of molybdenum-rich catalysts, are easily understood on the basis of the polymeric octahedral nature of the active surface sites in oxidized samples (*1*). The almost complete disappearance of absorption in the 270–330 nm region in the reduced samples indicates a profound reorganization of the catalyst surface with numerous ruptures of bridged oxygen bonds in the polymeric chain and leading to considerable amounts of Mo(IV), just as in the case of MoO_3. To explain the presence of some Mo(V) (see secondary peaks in Fig. 3), rupture of bridged oxygen bonds at preferential positions or different precursors are possible. The observation that under the milder conditions of outgassing Mo(V) is the only reduced species formed, favors the first proposition; moreover, similarity of results from outgassing and reduction experiments (Tables 3a, b) indicate similar Mo-surface complexes, with Mo(V) either in the form of $Mo_4O_{10}(OH)_2$ or as reduced heteropolyacids (Table 5). Their formation is rationalized if we recall the polymeric octahedral species present

in oxidized samples. As, however, these species are diamagnetic (*29*), the observed EPR signal (Fig. 3) cannot be well understood. A plausible explanation follows from the consideration that the progressive increase in MoO_3 content affects not only the geometry of coordination of supported species but also the acid-base characteristics of the support. To understand changes in the acid-base characteristics, consider progressive depletion of OH-groups as the amount of MoO_3 increases: upon dehydration one may expect creation of pair and triplet defects on the support, which should constitute strong acid sites at the unusually exposed aluminum ions (*30*). Cation vacancies such as oxide ions missing from regular surface oxide domain sites may also coexist and these should also be very strongly acidic (*31*). The increasing acidity of the support with progressive removal of OH-groups should in turn affect the acid-base character of Mo-oxo-species: if these changes are similar to those found in acid solutions (32), then MoO^{3+} is expected at the highest acid concentrations, followed by $[Mo_2O_3]^{4+}$ and $[Mo_2O_4]^{2+}$ at lower acidity. Amongst these, only MoO^{3+} is paramagnetic and this species may account for the observed ESR signal. This view complies well with previous evidence of the presence of MoO^{3+} on η-Al_2O_3 (*5*) and with the lower Mo(V) threshold on η-Al_2O_3 compared to γ-Al_2O_3 (*6*), which differs from η-Al_2O_3 by its acidity (*33*,*34*). We thus propose local formation of structures arising from interaction of MoO^{3+} and AlO^-, with Mo(V) in the role of a cation, as in $MoOPO_4$ (*35*). In this respect, we recall the results of Sultanov *et al.* (*10*) who reported a maximum concentration of Mo(V) at Al/Mo = 1 for coprecipitated $MoO_3 \cdot Al_2O_3$ samples outgassed at 600°C; the observed anisotropic factors ($g_\perp = 1.93$, $g_{||} = 1.88$), very close to our values, were interpreted as due to interaction of the axial oxygen of $[MoO_6]$ octahedra with the electron-acceptor Al-oxide centers (Lewis acid centers). Al ions thus appear to play a primary role in the process of stabilization of Mo(V).

REFERENCES

1. Giordano, N., Bart, J. C. J., Vaghi, A., Castellan, A., and Martinotti, G., *J. Catal.* **36,** 81 (1975).
2. Giordano, N., Vaghi, A., Bart, J. C. J., and Castellan, A., *J. Catal.*, in press.
3. Giordano, N., Padovan, M., Vaghi, A., Bart, J. C. J., and Castellan, A., *J. Catal.*, in press.
4. Hersch, P. A., *Anal. Chem.* **3,** 1031 (1960).
5. Seshadri, K. S., and Petrakis, L., *J. Phys. Chem.* **74,** 4102 (1970).
6. Dufaux, M., Che, M., and Naccache, C., *J. Chim. Phys. Physicochim. Biol.* **67,** 527 (1970).
7. Boreskov, G. K., Dzisko, V. A., Emelyanova, V. M., Pecherskaya, Yu. N., and Kazanskii, V. B., *Dokl. Akad. Nauk SSSR* **150,** 829 (1963).
8. Maksimovskaya, R. I., Anufrienko, V. F., and Kolovertnov, G. D., *Kinet. Katal.* **9,** 1186 (1968).
9. Peacock, J. M., Sharp, M. J., Parker, A. J., Ashmore, P. G., and Hockey, J. A., *J. Catal.* **15,** 379 (1969).
10. Sultanov, A. S., Talipov, G. Sh., Inoyatov, N. Sh., Tatarskii, V. P., and Samigov, K. A., *Kinet. Katal.* **12,** 1259 (1971).
11. Asmolov, G. N., and Krylov, O. V., *Kinet. Katal.* **11,** 1028 (1970).
12. Ashley, J. H., and Mitchell, P. C. H., *J. Chem. Soc. (A)* 2821 (1968).
13. Asmolov, G. N., and Krylov, O. V., *Kinet Katal.* **13,** 188 (1972).
14. Mitchell, P. C. H., and Williams, R. J. P., *J. Chem. Soc.* 4570 (1962).
15. Mitchell, P. C. H., and Trifiro, F., *J. Chem. Soc. (A)* 3183 (1970).
16. Papacontantinon, E., and Pope, M. T., *Inorg. Chem.* **9,** 667 (1970).
17. Larson, M. L., and Moore, F. W., *Inorg. Chem.* **2,** 881 (1963).
18. Gebrke, H., and Veal, J., *Inorg. Chim. Acta* **3–4,** 623 (1969).
19. Dunn, T. M., *in* "Modern Coordination Chemistry" (J. Lewis and R. G. Wilkins, Ed.), p. 292. Wiley (Interscience), New York, 1960.
20. Castellan, A., Bart, J. C. J., and Giordano, N., unpublished results.
21. Porter, V. R., White, W. B., and Roy, R., *J. Solid State Chem.* **4,** 250 (1972).
22. Clark, J. H., *J. Chem. Soc.* 417 (1964).
23. Dunne, T. G., and Cotton, F. A., *Inorg. Chem.* **2,** 263 (1963).

24. Masson, J., and Nechtschein, J., *Bull Soc. Chim. Fr.* 3933 (1968).
25. Ishii, Y., and Matsuura, I., *Technol. Rep. Kansai Univ.* **10,** 47 (1969).
26. Naccache, C., Bandiera, J., and Dufaux, M., *J. Catal.* **25,** 334 (1972).
27. Dollimore, D., and Rickett, G., Proc. 3rd I.C.T.A. Davos 1971, *in* "Thermal Analysis" (H. G. Wiedemann, Ed.), p. 43. Birkhauser Verlag, Basel, 1972.
28. Kazanskii, V. B., *Kinet. Katal.* **11,** 455 (1970).
29. Kriss, E. E., Rudenko, V. K., and Yatsimirskii, K. B., *Russ. J. Inorg. Chem.* **16,** 1146 (1971).
30. Peri, J. B., *J. Phys. Chem.* **69,** 220 (1965).
31. Eucken, A., *Disc. Faraday Soc.* **8,** 128 (1950).
32. Mitchell, P. C. H., *Quart. Rev.* **20,** 103 (1966).
33. MacIver, D. S., Tobin, H. H., and Barth, R. T., *J. Catal.* **2,** 485 (1963).
34. MacIver, D. S., Wilmot, W. H., and Bridges, J. M., *J. Catal.* **3,** 502 (1964).
35. Kierkegaard, P., and Westerlund, M., *Acta Chem. Scand.* **18,** 2217 (1964).